



Soil-structure interaction effects on the seismic response of a public building in Lefkas, Greece

Christos Karakostas¹ · Konstantinos Morfidis¹ · Emmanouil Rovithis¹ · Nikolaos Theodoulidis¹

Received: 18 July 2021 / Accepted: 5 November 2021 / Published online: 18 November 2021
© Springer Nature B.V. 2021

Abstract

An investigation of Soil-Structure Interaction (SSI) effects on the seismic response of the Regional Administration building in the island of Lefkas, Greece is performed, based on earthquake recordings from two accelerometric stations installed at the basement of the building and on ground surface at a certain distance from the structure, representing a free-field station. The observed deviation between basement and free-field records is explored by means of a hybrid numerical—analytical formulation in the framework of the substructure approach. To this end, the kinematic part of the interaction mechanism is modeled through commonly employed analytical transfer functions between ground surface and foundation base, while a detailed 3D mass-distributed Finite Element model is analyzed under both fixed and flexible supports to explore the seismic response of the building, as affected by inertial SSI effects. The comparison between predicted and recorded response shows a kinematic dominated response of the foundation that is characterized by strong filtering of the free-field motion at ground surface. Accordingly, various repercussions due to the potential underestimation of the seismic hazard from recording stations housed at the basement of buildings are discussed. Numerical results demonstrate also that soil compliance may have an important effect on the seismic demand quantified in terms of interstorey drifts of the building. Finally, a simplified MDOF lumped-mass stick model of the superstructure is also analyzed under flexible-base conditions, leading to a substantial overprediction of interstorey drifts compared to the 3D model.

Keywords Soil structure interaction · Substructure approach · Instrumented structures · Seismic analysis · Finite element model · Seismic hazard · Risk assessment

✉ Christos Karakostas
christos@itsak.gr

Extended author information available on the last page of the article

1 Introduction

Seismic analysis of structures is commonly performed by considering the structure fixed at its base and excited by the free-field motion at ground surface. Such assumptions disregard the interaction between the structure, its foundation and the supporting soil that takes place during earthquake shaking and may affect substantially both the vibrational characteristics and the base excitation of a compliant-base superstructure, compared to its fixed-base counterpart, especially in the case of stiff foundation-structure systems in soft soils. In particular, Soil-Structure Interaction (SSI) may modify the dynamic response of the system by (Veletsos and Meek 1974; Bielak 1975; Mylonakis et al. 2006 among others): (1) elongating the fundamental period of the structure; (2) mobilizing additional energy dissipation mechanisms in the form of soil hysteretic action and radiation of seismic waves emanating from the foundation; and (3) modifying the base motion that actually excites the structure with respect to the free-field motion at ground surface, which is usually associated to the filtering of the high-frequency components of the incident wave field within the building footprint and/or over the foundation depth in the case of embedded foundations, mainly due to the inability of a stiff foundation to follow soil deformations characterized by short wavelengths (Elsabee and Morray 1977; Veletsos et al. 1997; Stewart 2000; Kim and Stewart 2003; Conti et al. 2017, 2018).

From a computational point of view, a convenient manner to assess SSI effects is the substructure method, which considers the dynamic response of the coupled soil-foundation-structure system as the superposition of two analysis stages, reflecting accordingly two concurrent phenomena (Kausel et al. 1978; Makris et al. 1996; Gazetas and Mylonakis, 1998). First, a *kinematic* interaction analysis is performed, where both the foundation and the structure are considered massless, in order to derive the Foundation Input Motion (FIM) that is actually imposed at the base of the structure. In this regard, FIM may be different from the free-field motion at ground surface and may also include a rotational component. Second, an *inertial* interaction analysis, which refers to the response of the complete SSI system to D'Alembert forces associated with the FIM excitation and it may be performed in two steps: (1) model the complex-valued dynamic stiffness and damping of the soil-foundation system through springs and dashpots for each mode of vibration of the foundation and (2) obtain the seismic response of the structure and foundation supported on these springs and dashpots and subjected to the FIM.

The inertial-induced lengthening of the structural period due to SSI is usually considered to be beneficial in terms of the seismic loading imposed on a compliant-base structure, but may also be detrimental under certain seismic and soil conditions, depending primarily on the elastic response spectrum at the ground surface and the dynamic characteristics of the structure (Mylonakis and Gazetas 2000). On the other hand, the kinematic-induced modification of the base motion may be beneficial, leading to a lower seismic demand with respect to the free-field motion, especially for stiff and embedded foundation configurations (e.g. Conti et al. 2018; Di Laora and de Sanctis 2013; Iovino et al. 2019). The issue has been recognized by design codes, some of which provide analytical formulae to consider kinematic effects on the seismic loading of structures (ATC 2005; ASCE 2007; NIST 2012). However, larger spectral amplitudes of the foundation motion over the free-field motion have also been reported by means of earthquake records from instrumented buildings (Poland et al. 2000, Pandey et al. 2012). It is noteworthy that the above studies reported different trends in the longitudinal and the transverse direction of the same structure, referring to either attenuation or amplification of the base slab motion with respect to

the free-field surface motion under the same earthquake. It should be noted though that in a real instrumented structure, the foundation motion is inherently affected by both kinematic and inertial interaction. However, the contribution of the inertial interaction stemming from the oscillation of the superstructure is primarily concentrated near the fundamental, flexible-base frequency of the structure, which allows the identification of kinematic effects from records at building basements at mainly high frequencies that may be far from the SSI frequency of the structure (Stewart 2000; Trifunac et al. 2001; Kim and Stewart 2003; Givens et al. 2012) and the validation of relevant numerical or analytical models (Conti et al. 2018; Sotiriadis et al. 2019, 2020).

Under the hypothesis of linear behavior for all the components of the SSI system, which allows a rigorous implementation of the substructure approach due to the associated principle of superposition, this paper explores SSI effects by means of a low-intensity earthquake recorded at the basement of an instrumented building and at the ground surface at a certain distance from the building, representing free-field conditions. First, the available records at the two locations are compared in both time and frequency domain to identify records-based SSI effects, referring primarily to the kinematic-induced modification of the free-field motion. A detailed 3D Finite Element model is then employed to model the superstructure under both fixed and flexible supports to investigate inertial SSI effects. To this end, a modal analysis of the 3D FE model is performed, followed by a time-domain analysis to derive structural response features, referring to acceleration time-histories at the location of the sensor at the building basement and interstorey drift ratios, as affected by SSI. The Foundation Input Motion, computed from published analytical expressions of relevant transfer functions, and the recorded free-field motion are employed as base excitations to assess the role of the kinematic-induced modification of the free-field motion on structural response. With reference to the flexible-base structure excited by the FIM, the response of the 3D FE model is compared to a simplified Multi-Degree-of-Freedom (MDOF) stick model of the building, following up on an earlier study of the authors (Karakostas et al. 2017). The performance of alternative, code-allowed considerations for the excitation motion at the base and the fixity conditions of the structure is explored regarding the reliability of the estimated seismic response in each case. The effect of SSI on the modal characteristics of the specific building is also discussed during interpretation of the building's response under earthquake loading.

2 Description of the building and available records

The structure under study refers to the Regional Administration building in the town of Lefkada, Greece (Fig. 1) that was excited by the M6.1 Cephalonia earthquake mainshock of 26-1-2014. This earthquake was related to the Cephalonia transform fault zone, with a dextral strike slip causative fault (Theodoulidis et al. 2016).

At the basement of the building a broad band accelerograph with a high resolution 24-bits digitizer (CMG-5TDE, Güralp[®]) was installed by ITSAK as part of the National Accelerometric Network and recorded the mainshock (station LEF2). At a distance of about 70 m away from the building, a second accelerograph was also installed (station LEF3), which is considered as representative of free-field conditions (Fig. 1, right).

The comparison of the acceleration recordings of the 26-1-2014 event shows that the amplitudes of the recorded responses at the free-field sensor are higher than those at the building basement (Fig. 2a), while the frequency content of the free-field recordings is



Fig. 1 The Lefkada Regional Administration building (yellow ellipse) and location of the free-field accelerometer (yellow arrow)

richer, especially in the 3 to 6 Hz range (Fig. 2b). The differences between the corresponding elastic response spectra (5% critical damping ratio) are shown in Fig. 2c. It is noted that the recordings (originally in N–S and E–W directions) were appropriately rotated to align with the building’s longitudinal (x – x) and transverse (y – y) directions.

The structure under investigation is a statically independent part of a five-building complex (Fig. 3a, shaded part III), which was constructed in 2009. The initial design (of June 1991), was revised in August 2007, and the building conforms to the 2000 Greek R/C Code (EKOS2000 2000) as well as the 2000 Greek Seismic Code (EAK2000 2000) and their subsequent amendments.

The building consists of a basement, ground and first floor (Fig. 3b). Each floor has an area of 761m², and the height is 3 m at the basement and 3.25 m at the other two floors. There is also an inner central court of 114.95m² area (cross-lined area at Fig. 4a). The formworks of the building slabs are presented in Fig. 4a and that of the strip foundation in Fig. 4b. The location of the high-accuracy sensor at the building basement is shown with a red dot in Fig. 4b.

3 Development of a 3D numerical (F.E.) model of the building

As already mentioned, a full 3D finite element model of the building was developed (Fig. 5). This allows the computation of the building response at the exact location of the sensor at its basement that recorded the 26–1–2014 event and hence a reliable comparison between the recorded and computed response. The characteristics and the assumptions used for the modeling of the building are described in the following.

The model was formed by using the beam/column and shell elements of the SAP2000 (©Computers & Structures Inc.) structural analysis program. In the modeling of R/C vertical members and beams, the axial as well as the shear deformations were taken into account (the dimensions of the cross-sections of these members are presented in Fig. 6, where columns and shear walls are denoted with letter K and beams with letter Δ). No reduction of the bending/axial stiffness was assumed (such as those prescribed by the Seismic Code for the design earthquake), due to the low intensity of the examined event. The concrete was modeled as an isotropic linear elastic material with elastic Young’s modulus $E=3.1E7$ kN/m², Poisson ratio $\nu=0.2$ and unit weight $\gamma=25$ kN/m³. A critical damping ratio of 3.5% was assumed for the viscous damping, as proposed in Dai et al. 2020 for low intensity (i.e. $PGA < 0.1$ g) earthquakes. We note that the corresponding Seismic code-prescribed value for R/C buildings is 5% for the design earthquake.

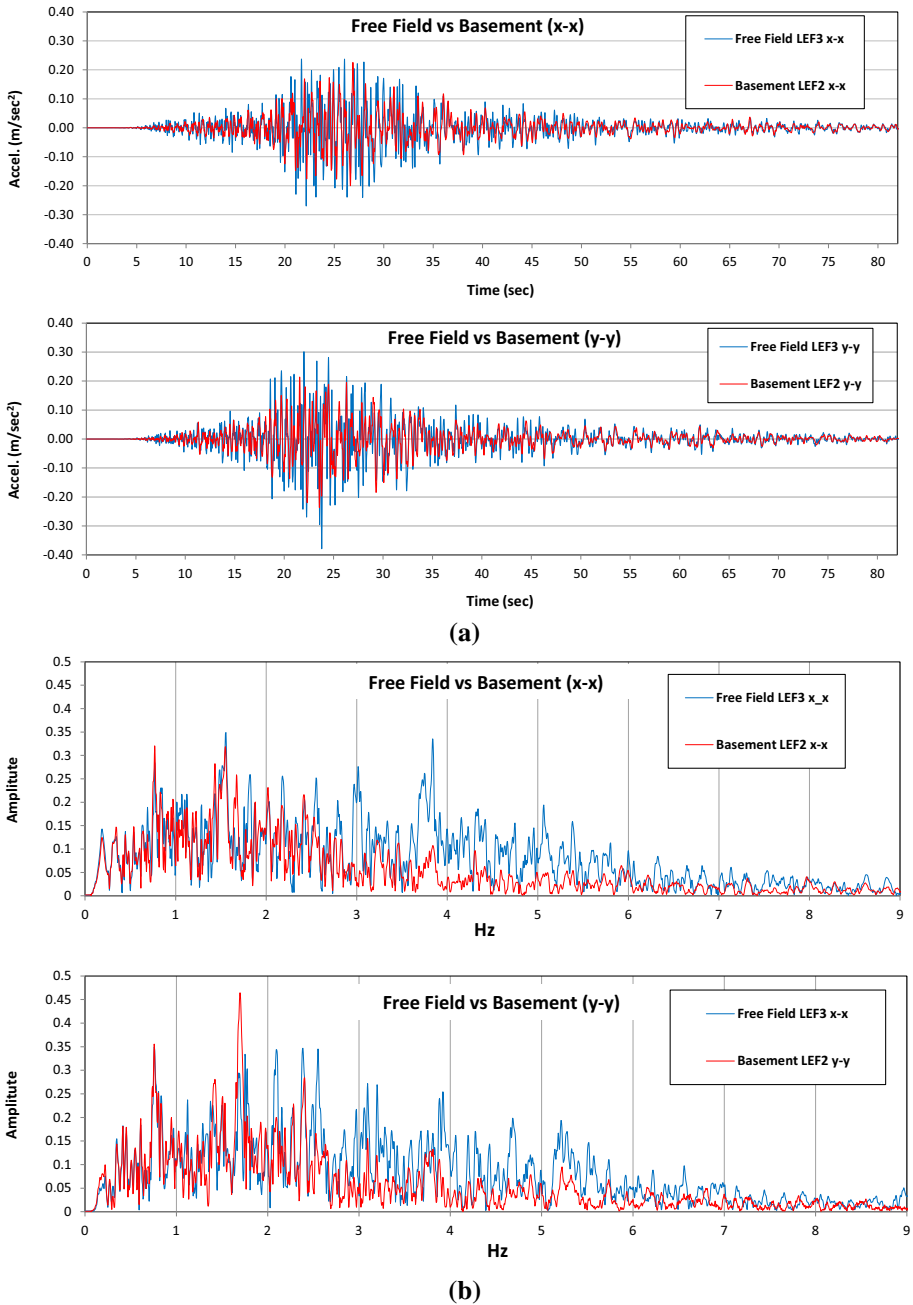


Fig. 2 Recordings of the Cephalonia 26–1–2014 earthquake at free-field conditions (blue) and at the basement of the building (red) along the longitudinal (x–x) and transverse (y–y) directions of the building: **a** acceleration time histories **b** Fourier amplitude spectra **c** 5%–damped elastic response acceleration spectra

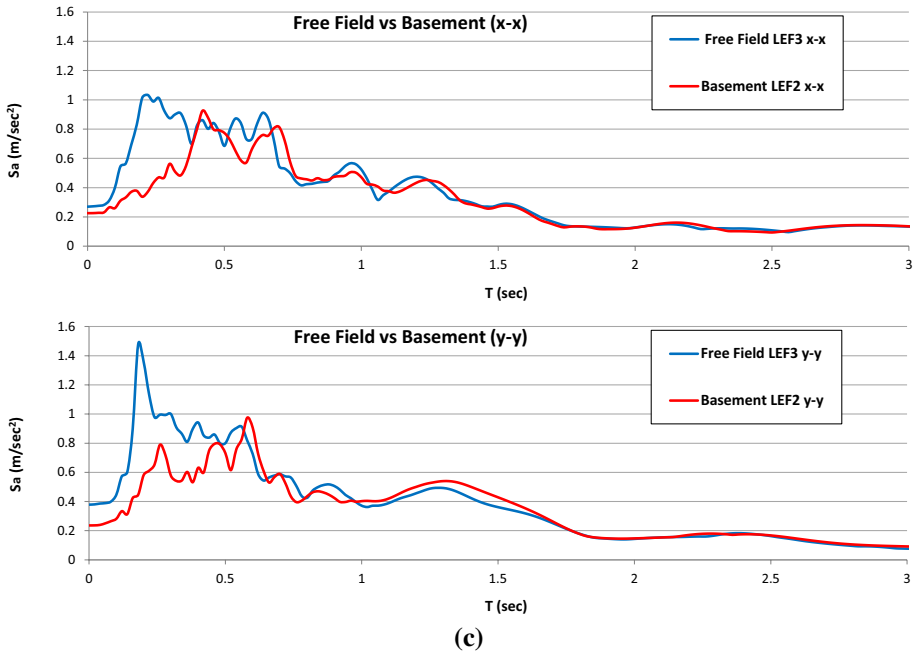


Fig. 2 (continued)

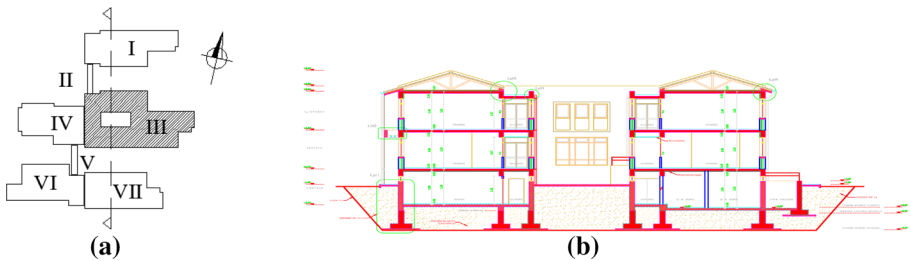


Fig. 3 **a** Plan view of the Lefkada Administrative Complex **b** Height cross-section of building III

All the floor slabs of the building have the same shape. Due to the fact that this is an irregular shape with a big aspect ratio and a relatively large internal opening (Fig. 7), the floor slabs were modelled with thin-type shell elements (e.g. Avramidis et al. 2016), instead of using the—not a priori valid in the herein examined case—assumption of diaphragmatic behaviour. To this end, the aspect ratios of the shell elements correspond to a square shape, at the greatest feasible degree.

Moreover, shell elements were used for the modeling of the perimetric R/C wall at the basement of the building (Fig. 8). Classic beam/column elements were used to model the beam webs, noting that the corresponding flanges of the equivalent internal T-sections (or perimetric Γ -sections) are already modeled through the shell elements of the floor slabs. The vertical structural elements (columns and R/C walls) were also

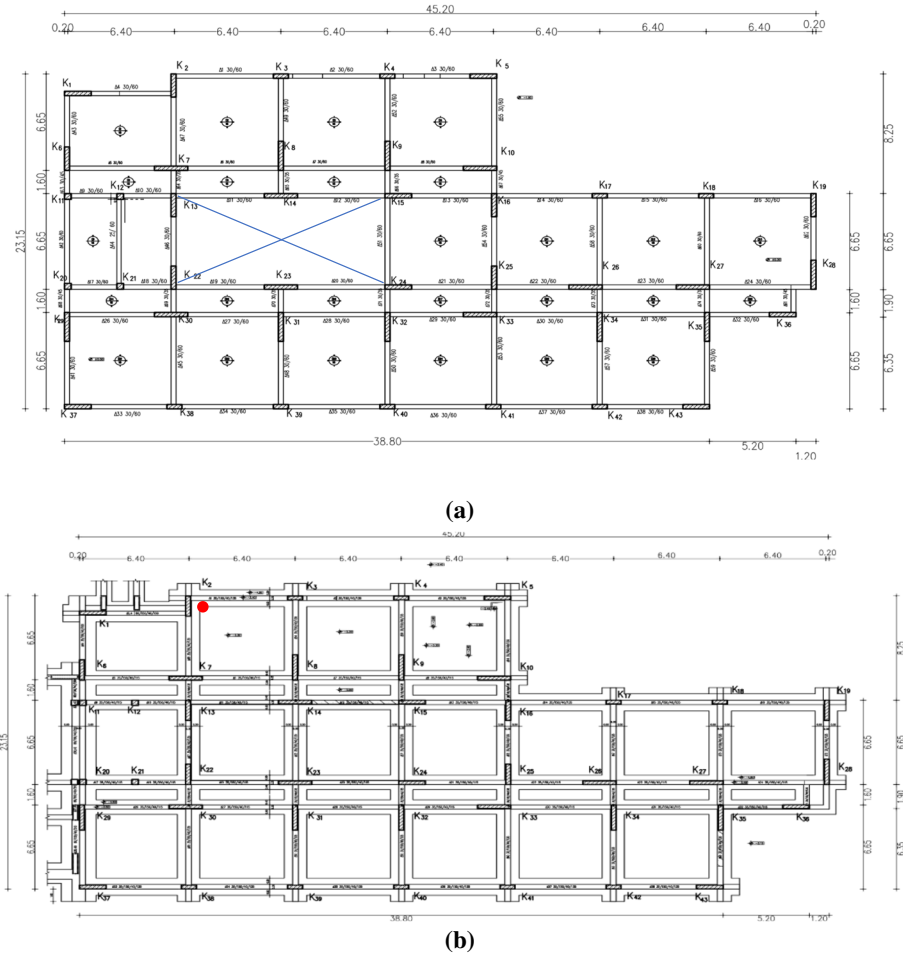
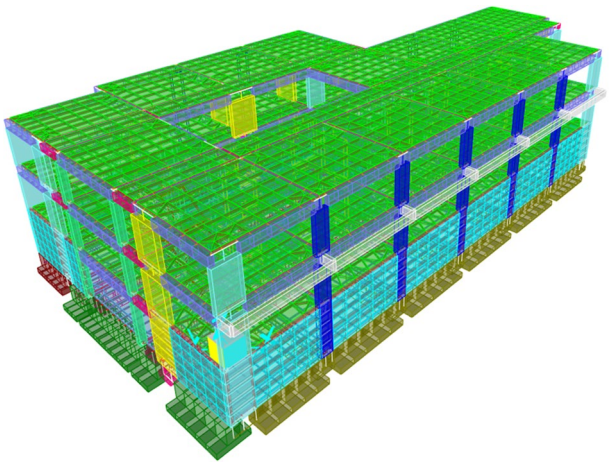


Fig. 4 Formworks of **a** a typical floor slab and **b** the foundation, with the location of the high-accuracy sensor at the basement slab (red dot)

Fig. 5 3D F.E. model of the building



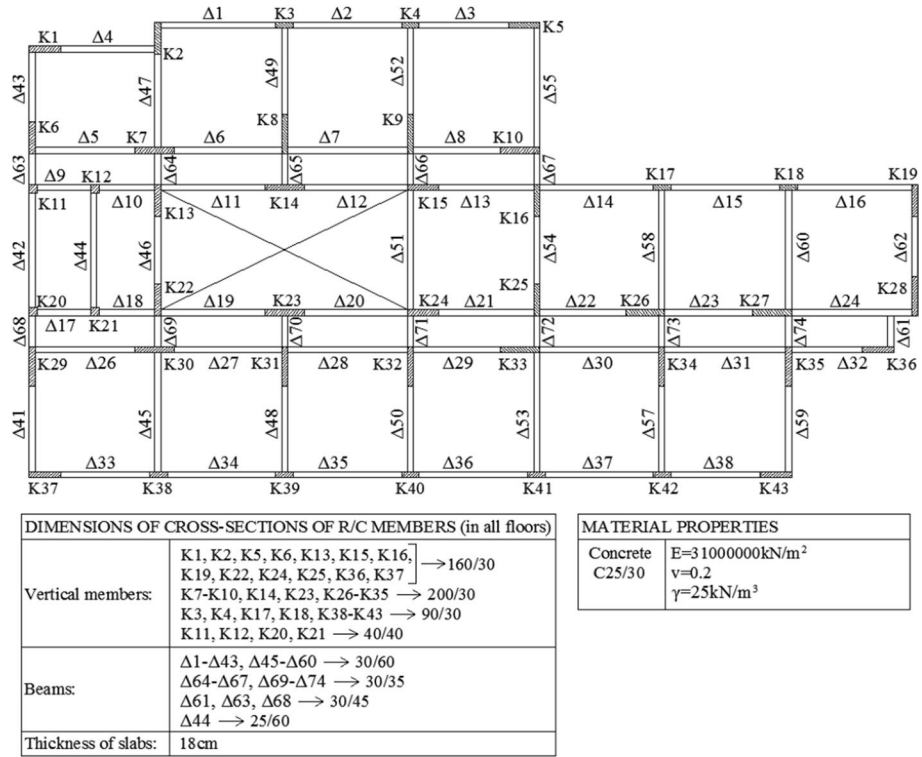
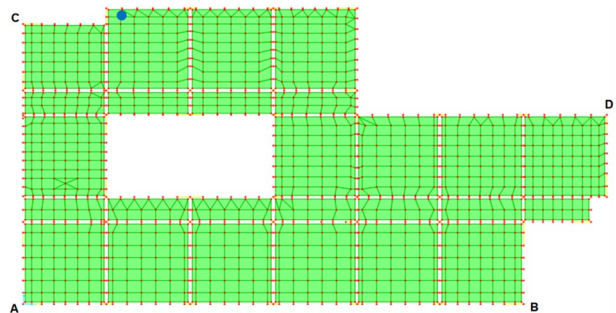


Fig. 6 Geometric and material data for the building model

Fig. 7 Discretization of the basement slab of the building using shell elements. The joint at the location of the accelerograph is denoted with the blue donut. Corner joints of the building where interstorey drift ratios are evaluated are denoted with letters A...D



modeled using beam/column elements. For the simulation of the joints of vertical elements and beams (which behave as rigid bodies) rigid beam/column elements were used.

The modeling of the foundation required a special attention since at the level of -3.5 m (i.e. below the ground surface) there is a slab on which the high-accuracy accelerograph inside the building is installed (blue dot in Fig. 7). This slab was also discretized by shell elements and a joint was introduced at the location of the accelerometer sensor, in order to compute its dynamic response during the 26-1-2014 seismic excitation. Below this slab

Fig. 8 Shell and beam/column elements used for modeling the building

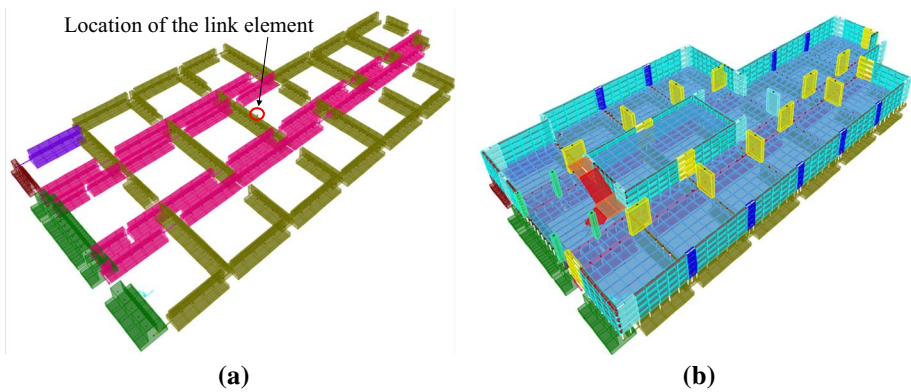
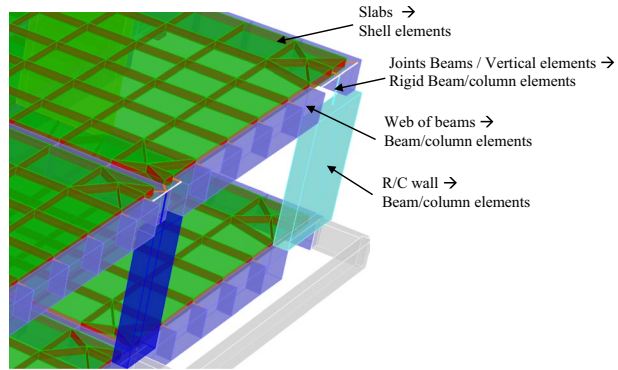


Fig. 9 Modelling of **a** the internal foundation beams and **b** the perimeteric foundation R/C walls

there is a strip foundation (Fig. 9a), with the bottom flanges of foundation beams sitting on the ground at the -4.475 m level. Thus, the modelling of the internal foundation beams was based on beam/column elements with reverse T-sections (Fig. 9a) whereas the modelling of the perimeteric ones was based on a combination of beam/column elements with a reverse T-section up to the -3.5 m level (where the lowest slab is located) and shell elements up to 0 m (ground) level, where is the top of the basement perimeteric R/C walls (Fig. 9b).

It must also be noted that in the model, a constraint (denoted as “body constraint” in SAP2000 2000), was applied to all joints at the -4.475 m level (i.e. at the bottom of the foundation beams), forcing them to move as a rigid 3D-body. This assumption is compatible to the rigid basement assumption used in order to take into account the SSI phenomena, as it is described later (see Sect. 4), and it is physically justified by the box-type basement of the building due to the large stiffness of the strip foundation beams, the RC slab at the -3.5 m level and the perimeteric RC basement walls. Flexible-base conditions of the superstructure were modeled through a link element introduced at the geometric mass center of the strip foundation at the -4.475 m level (Fig. 9a). For this reason, a special joint for the link element was inserted at this level, and the aforementioned “body constraint” was also applied to it. The link element consists of six separate “springs,” one for each of

six deformational degrees of freedom (DOFs), and each spring can in general be supplied with linear/nonlinear or frequency-dependent stiffness and damping properties. Interactions between the springs of different DOFs can also be taken into account (i.e. leading to full 6×6 stiffness and damping matrices). Details on the actual spring values used for the present investigations are given later in the paper (see Sect. 4.2).

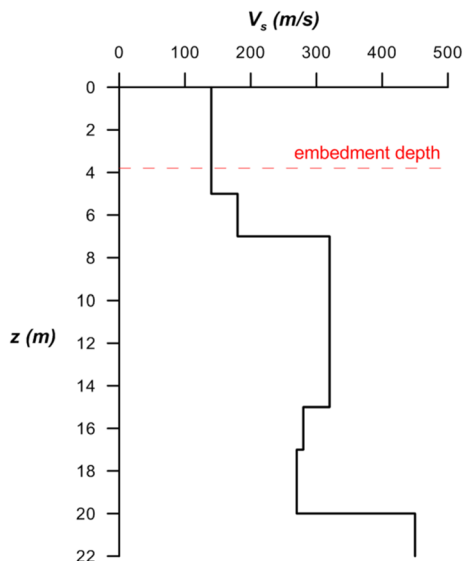
Finally, regarding the mass discretization of the building, it must be noted that the mass was suitably considered as distributed to all structural members, yielding the proper inertial forces at all 6 degrees of freedom of the model nodes. Apart from the dead loads, appropriate live loads were considered, compatible to the actual ones during the 26-1-2014 event. For live loads, the Greek Seismic Code prescribes nominal values of 2 kN/m^2 for internal slabs and 5 kN/m^2 for staircases and balconies, and for seismic design these loads are considered at 30% of these nominal values. Given the fact that the earthquake took place on Sunday, when the building was not fully operational, in the dynamic investigations of the present research effort live loads were assumed at 50% of the values prescribed by the Code for seismic design (i.e. at 15% of their nominal values).

4 Investigation of SSI effects on the seismic behaviour of the building

4.1 Foundation soil properties

Based on an available geotechnical borehole performed very close to the instrumented building under study (Sotiriadis et al. 2019), the foundation soil profile is formed by approximately horizontal layers and it is composed of a 1.5 m thick made ground (MG) followed by 2.5–3 m thick soft clays (CL) up to 4–5 m from the ground surface. Then, alternating layers of silty sands (SM) and clayey sands (CS) are met between 5 to 15 m approximately, which are underlain by stiffer clays. The corresponding shear wave propagation velocity profile is shown in Fig. 10 down to the depth of 22 m where data were available. The embedment depth of the foundation is also shown.

Fig. 10 Shear wave propagation velocity profile of the instrumented building's foundation soil



4.2 Foundation input motion

With reference to the kinematic part of the substructure approach, it has already been noted that an embedded foundation, due to its stiffness, may not always follow short wavelengths imposed by the surrounding soil, during the passage of seismic waves, and therefore the Foundation Input Motion (FIM) may be different from the free-field motion at ground surface by filtering high frequency components. Additionally, a rotational component of motion arises with no counterpart in free-field conditions. In order to quantify the above physical phenomenon, horizontal (I_u) and rotational (I_θ) kinematic interaction factors, relating the horizontal (U_{FIM}) and the rotational (θ_{FIM}) component of the Foundation Input Motion, respectively, with the free-field motion at ground surface (U_{ff0}) are defined as:

$$I_u = \frac{U_{FIM}}{U_{ff0}} \tag{1}$$

$$I_\theta = \frac{\theta_{FIM}H}{U_{ff0}} \tag{2}$$

Under the hypothesis of coherent shear waves propagating vertically, we employ the analytical expressions for I_u and I_θ proposed by Elsabee and Moray (1977):

$$I_u = \begin{cases} \cos\left(\frac{\omega H}{V_s}\right), & \omega \leq 0.7 \frac{\pi}{2} \frac{V_s}{H} \\ 0.453, & \omega > 0.7 \frac{\pi}{2} \frac{V_s}{H} \end{cases} \tag{3}$$

and

$$I_\theta = \begin{cases} 0.257 \frac{H}{B} \left[1 - \cos\left(\frac{\omega H}{V_s}\right) \right], & \omega \leq \frac{\pi}{2} \frac{V_s}{H} \\ 0.257 \frac{H}{B}, & \omega > \frac{\pi}{2} \frac{V_s}{H} \end{cases} \tag{4}$$

Notations in the above expressions follow those shown in Fig. 11. V_s may be interpreted as a time-averaged shear wave velocity over the embedment depth (H) of the foundation (Givens et al. 2012):

Fig. 11 Schematic definition of the free-field motion and the Foundation Input motion introduced in the definition of the kinematic interaction factors (modified after Conti et al. 2017)

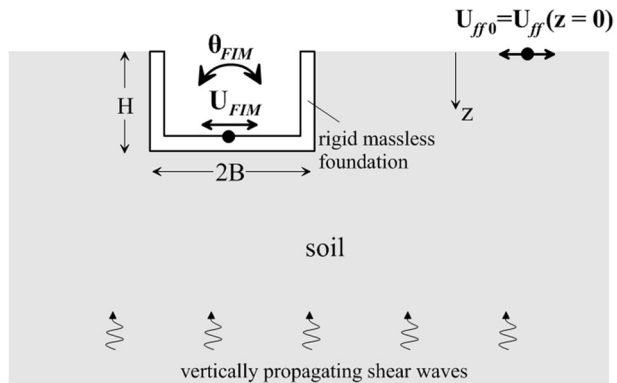


Fig. 12 Schematic graph of the plan view and cross-sections of the building’s foundation

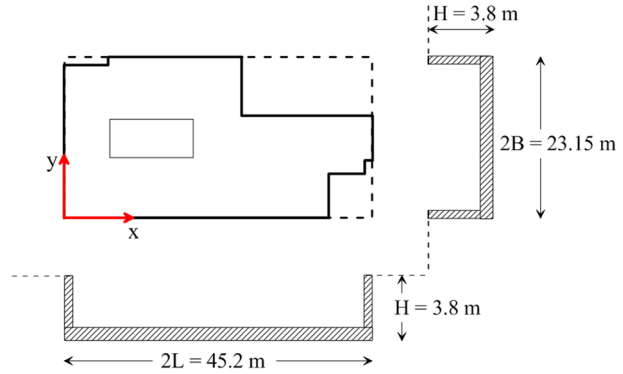
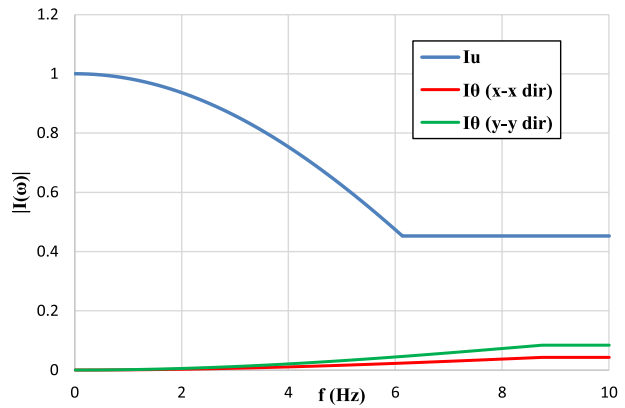


Fig. 13 Amplitude of kinematic interaction factors I_u and I_θ (Eqs. 3–4) employed to derive Foundation Input Motion



$$V_{s,avg} = \frac{H}{\sum_{i=1}^n \frac{\Delta Z_i}{V_{s(i)}}} \tag{5}$$

For the examined case study, $V_{s,avg}$ was taken equal to 140 m/s based on the shear wave velocity profile shown in Fig. 10, while the mass density (ρ) and the Poisson ratio of the soil were considered at 1.85 t/m³ and 0.3, respectively. Soil material damping may be incorporated in the above expressions by using the standard substitution $V_s \rightarrow V_s^* \cong V_s(1 + iD)$, where D corresponds to the hysteretic damping ratio of the soil. A low-strain value at 5% was considered for the purpose of this investigation. Note also that the dimensions of the foundation employed for the derivation of the foundation dynamic stiffness (Fig. 12), correspond to a foundation width-to-embedment depth ratio of 11.9 and 6.1 along the X-axis and Y-axis, respectively. It should be noted that an embedment depth of 3.8 m was assumed, due to the fact that the basement slab of the building rests at this level on the webs of the strip foundation beams.

Upon implementing the above soil and foundation parameters, the amplitude of the kinematic interaction factors I_u and I_θ are plotted in Fig. 13 against frequency (f) of excitation.

Once the kinematic interaction factors have been obtained, the Foundation Input Motion can be derived in time domain for a given free-field motion at ground surface by

means of Fast Fourier and inverse Fast Fourier Transformations. With reference to the translational acceleration component $[\ddot{U}_{FIM}(t)]$ of the FIM, the above derivation is possible through the following expression:

$$\ddot{U}_{FIM}(t) = iFFT [I_u * FFT(\ddot{U}_{ff0}(t))] \tag{6}$$

A similar elaboration may be performed for the rotational kinematic interaction factor (Eq. 4) to derive the rotational component of the Foundation Input Motion. However, for the particular soil–foundation configuration, the rotational component is expected to be negligible, as reflected in the very low values of the associated interaction factor in the main frequency range of the free-field signal between 1 and 5 Hz (Fig. 13). The horizontal accelerations at the base of the foundation computed in time domain by Eq. (6) along the x–x and y–y directions of the building and the corresponding 5% damped elastic response acceleration spectra are shown in Fig. 14, in comparison with the respective free-field recordings, acquired from station LEF3.

4.3 Treatment of foundation stiffness

With reference to the inertial part of the substructure approach, soil compliance is modeled through point springs and dashpots attached to the base of the superstructure, the frequency-dependent properties of which reflect the dynamic stiffness and damping of the foundation and can be cast in the form of complex-valued impedance functions $\mathfrak{R}_{emb,j}(\omega)$ for any vibration mode (j) of the foundation (Gazetas 1991; Mylonakis et al. 2006):

$$\mathfrak{R}_{emb,j}(\omega) = \overline{K}_{emb,j}(\omega) + i\omega C_{emb,j}(\omega) \tag{7}$$

The dynamic stiffness of the foundation $\overline{K}_{emb,j}(\omega)$ is related to its static stiffness $K_{emb,st,j}$:

$$\overline{K}_{emb,j}(\omega) = K_{emb,st,j} k_{emb,j}(\omega) \tag{8}$$

through the dynamic stiffness coefficient $k_{emb,j}$ being in general frequency-dependent. The dashpot coefficient $C_{emb,j}(\omega)$ involves both radiation and hysteretic type of damping:

$$C_{emb,j}(\omega) = C_{emb,rad,j}(\omega) + C_{emb,hyst,j}(\omega) = C_{emb,rad,j}(\omega) + \frac{2\overline{K}_{emb,j}(\omega)\beta}{\omega} \tag{9}$$

In the above expressions, the subscript *emb* refers to an embedded foundation and ω is the cyclic frequency of excitation. Pertinent formulae for embedded foundations (Gazetas 1991; Mylonakis et al. 2006) were employed to derive springs and dashpots for the case of Lefkada building by assuming the whole foundation as fully embedded (embedment depth $H=3.8$ m, see Fig. 12). To this end, the foundation system was treated as rigid, taking into account the large bending stiffness of the grid beams, as well as the presence of the RC floor slab and the perimeter shear walls at the basement, which are expected to contribute substantially to the overall stiffness of the foundation system, as already mentioned above. A circumscribed rectangle of dimensions $2L \times 2B$ ($=45.2 \text{ m} \times 23.15 \text{ m}$), shown in Fig. 12 with a thick dashed line was considered for computing the impedance functions of the embedded foundation under study.

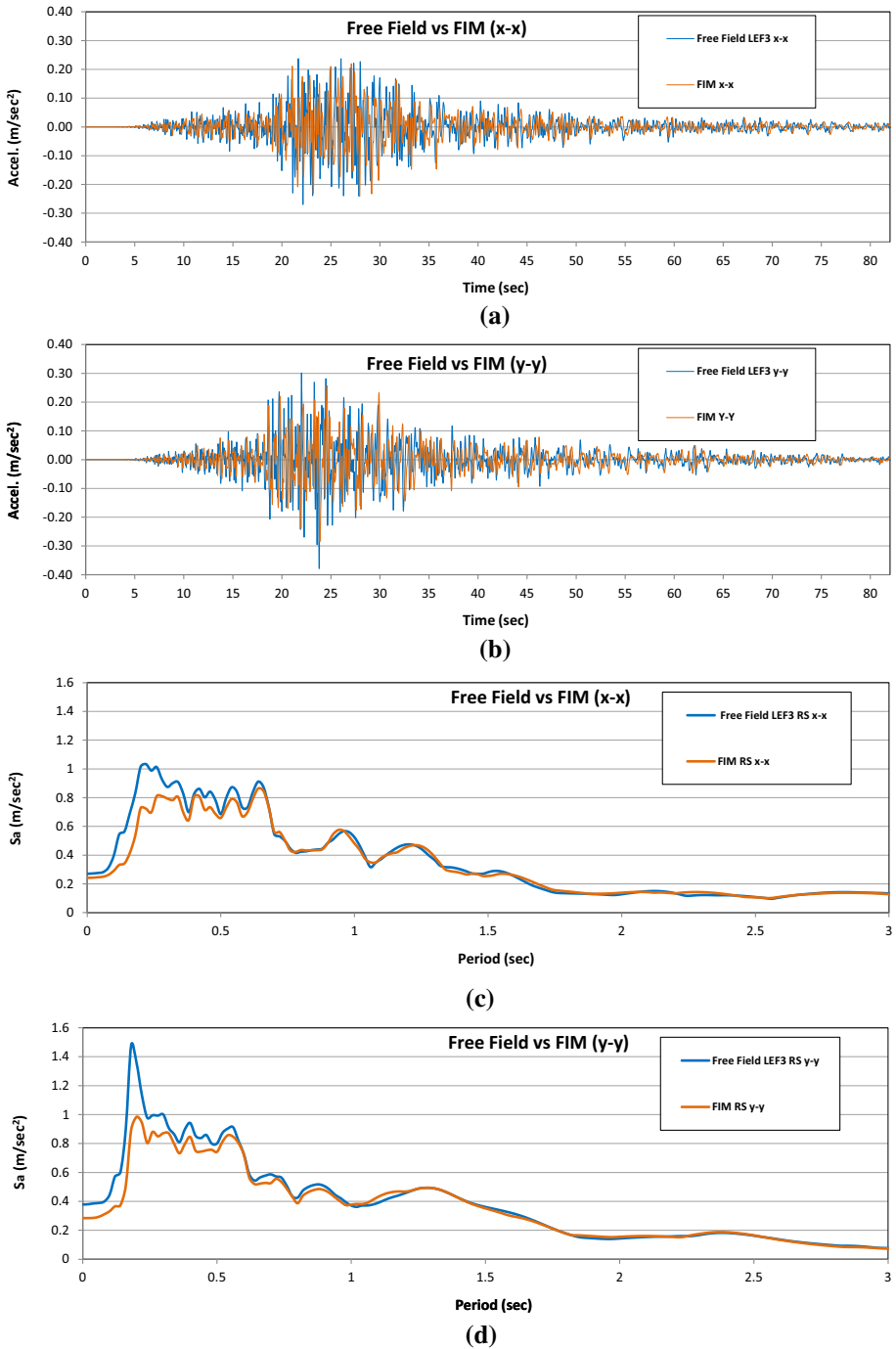


Fig. 14 Free-Field (station LEF3) recordings and derived Foundation Input Motions: **a, b** Acceleration time histories along the (x-x) and (y-y) directions **c, d** corresponding 5% damped elastic response acceleration spectra

As an example, following the notations in the above references, the static stiffness ($K_{emb,st,rx}$) corresponding to the rocking vibration mode of the foundation about the longitudinal ($x-x$) axis is given by the formula (Gazetas 1991; Mylonakis et al. 2006):

$$K_{emb,st,rx} = K_{surf,st,rx} \left\{ 1 + 1.26 \frac{d}{B} \left[1 + \frac{d}{B} \left(\frac{d}{H} \right)^{-0.2} \left(\frac{B}{L} \right)^{0.5} \right] \right\} \tag{10}$$

where $d=H$ due to the assumption of the foundation being fully embedded and $K_{surf,st,rx}$ refers to the corresponding static rocking stiffness of a surface foundation with the same plan dimensions, which may be computed from (Gazetas 1991; Mylonakis et al. 2006):

$$K_{surf,st,rx} = \frac{G}{1-\nu} I_{bx}^{0.75} \left(\frac{L}{B} \right)^{0.25} \left(2.4 + 0.5 \frac{B}{L} \right) \tag{11}$$

where I_{bx} is the area moment of inertia of the foundation-soil contact surface around x axis, G is the shear modulus of the foundation soil. The associated dynamic stiffness coefficient $k_{emb,rx}(\omega)$ is given by (Gazetas 1991; Mylonakis et al. 2006):

$$k_{emb,rx}(\omega) = 1 - 0.2 \left(\frac{\omega B}{V_s} \right) \tag{12}$$

in order to derive the dynamic stiffness $\bar{K}_{emb,rx}(\omega)$ from Eq. (8). Corresponding expressions from the above references were employed to compute the dynamic stiffness of the foundation for the other modes of vibration, the associated radiation dashpot coefficients $C_{emb,rad,j}(\omega)$ and eventually derive the overall damping coefficient $C_{emb,j}(\omega)$ in Eq. (9). Given the low amplitude of the recorded free-field acceleration at 0.03 g (Fig. 2), the above calculations were performed for a shear modulus (G) of the soil equal to its low-strain value within the embedment depth. It is reiterated that the Poisson ratio (ν) of the soil was considered equal to 0.3. The mean cyclic frequency $\omega_m (= 2\pi f_m)$ defined in Rathje et al. 1998 as:

$$\omega_m = 2\pi \frac{\sum_i C_i^2}{\sum_i C_i^2 \left(\frac{1}{f_i} \right)} \tag{13}$$

was adopted as an index of the frequency content of Foundation Input Motion, in order to obtain a single complex value of the foundation impedance functions, following a similar consideration in Makris et al. 1996 for the case of a bridge pier founded on piles. This particular choice was considered more relevant for the problem at hand as our intention was not to derive the properties of a replacement simple oscillator (Veletsos and Meek 1974) for the examined building, that would necessitate the use of the SSI frequency (computed iteratively) for the computation of the foundation stiffness. In Eq. (13), C_i refer to the Fourier amplitudes of an acceleration time history and f_i are the discrete Fourier transform frequencies between 0.25 Hz and 20 Hz. Upon applying Eq. (13) for the horizontal acceleration time history of the Foundation Input Motion computed earlier, a mean frequency f_m at approximately 1.6 Hz was derived for both $x-x$ and $y-y$ directions of excitation. This value was then employed to compute the properties of the point springs and dashpots of the link element (described in Sect. 3) attached to the base of the 3D F.E. model (denoted as SAP CVLink—Constant Value Link—model), including a cross swaying-rocking stiffness term due to the foundation embedment, to account for the compliance of the foundation soil.

5 Results of the numerical investigations

5.1 Analytical results using the detailed 3D F.E. building model

Figure 15 shows the comparison between the recorded excitation by the sensor at the basement of the building (station LEF2) and the one computed at the same location by the 3D finite element model, both in time and frequency domain. It can be seen that the predicted response is acceptably similar, from an engineering point of view, to the actual one in the time domain, while Fourier amplitudes are overpredicted for frequencies above 2 Hz approximately, denoting a richer energy content in the high-frequency range with respect to the recorded motion. In order to explore the above deviation, the available earthquake records were further processed to derive the amplitude of the foundation-to-free-field transfer function amplitude in the form:

$$|H_1| = |S_{ab}(f)/S_{aa}(f)| \quad (14)$$

where $S_{aa}(f)$ represents the auto power spectral density functions of the free-field motion (i.e. LEF3 station record), while $S_{ab}(f)$ is the cross power spectral density function between the free-field and the foundation motion (i.e. LEF2 station recording). To this end, the smoothing procedure described in Conti et al. 2018 was followed to derive $|H_1|$, upon satisfying certain criteria for high-coherence data points to identify noise-dominated frequencies (Kim and Stewart 2003; Mikami et al. 2008; Givens et al. 2012). The $|H_1|$ function in Eq. (14) was computed separately from the records along the x - x and the y - y direction of the building. These records-based curves are compared in Fig. 16 with the amplitude of I_u (Eq. 3). Despite the elaboration of a single record that certainly disallows generalization, it may be observed clearly that, for the particular combination of the examined SSI system and earthquake motion, the analytical expression of I_u underestimates substantially the strong kinematic-induced filtering effect of the foundation for frequencies that are again above 2 Hz. It should be noted that the records-based function of $|H_1|$ may also involve inertial-induced effects that are normally reflected in an oscillating trend of the transfer function with values above unity close to the first natural frequency of the SSI system. However, such a trend is not easily recognizable in Fig. 16, while kinematic effects are expected to prevail with increasing frequency. This provides support that the deviation between records and numerical predictions in Fig. 15 should primarily stem from the underestimation of the filtering effect by Eq. 3, indicating a dominant kinematic effect on the actual response of the foundation.

In order to quantify the differences between the computed and the recorded response at the LEF2 station at the basement of the building, some ground motion parameters that represent the potential of an excitation to inflict structural damage (e.g. Kramer, 1996) are presented in Table 1. The corresponding parameters are also presented for the recorded response at the free-field station LEF3.

From the parameter values presented in Table 1, it can be seen that the predicted response at the basement of the building, taking into account SSI effects, overestimates in general the recorded one, but within an acceptable degree from an engineering point of view. The free-field recording, on the other hand, has a higher potential for structural damage. Among the parameters of Table 1, the maximum peak ground acceleration (PGA) is the one currently adopted by the majority of Seismic Codes (including the Greek one) for the seismic design or seismic capacity evaluation of buildings. The Greek Seismic Code also allows to consider the building fixed at its base (i.e. ignoring SSI effects). It should

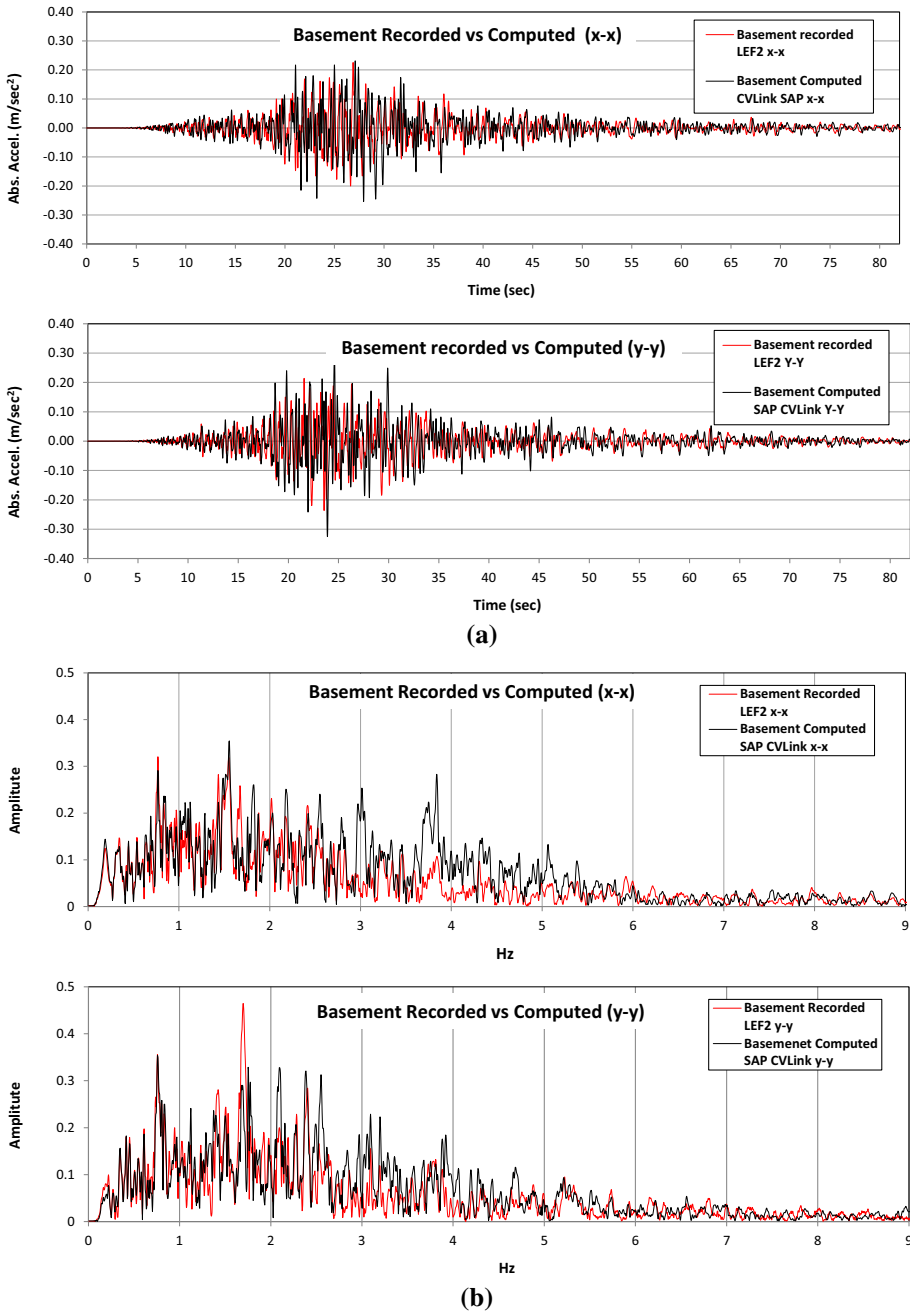
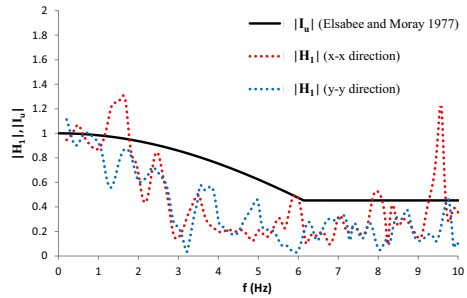


Fig. 15 Comparison between actual recording at the basement (station LEF2, in red) and analytical prediction at the same location considering the SSI effects (SAP CVlink assumption) (black) **a** in time and **b** in frequency domain

Fig. 16 Comparison of records-based transfer function $|H_i|$ between basement (LEF2) and free-field (LEF3) recordings with the analytical expression I_u proposed by Elsabee and Moray



be noted that in several countries (including Greece), a substantial number of recording stations as part of national accelerometric (strong-motion) networks are housed, for practical reasons, at the basement of structures, and not in free-field conditions, and the Greek Seismic Code does not explicitly impose any restriction for the direct use of their recordings, in lack of actual free-field ones. Actually, as previously described, the station LEF2 at the basement of the building under investigation is such a station of the National Strong-Motion network. In view of this issue, we made a parametric investigation of the building response, by comparing the maximum interstorey drift ratios under three modeling cases, all compatible to the Greek Seismic Code provisions:

- Case 1: Fixed-base structure excited by the free-field motion recorded by the LEF3 station.
- Case 2: Fixed-base structure excited by the basement motion recorded by the LEF2 station
- Case 3: Flexible-base structure excited by the Foundation Input Motion.

The corresponding analysis results in terms of maximum interstorey drift ratios (MIDR) at four corner joints (A, B, C, D) of the building (Fig. 7) are presented in Table 2. With reference to a vertical element of a storey, these ratios were computed by:

$$MIDR = \frac{\max |u(t_i)^T - u(t_i)^B|}{h} \tag{15}$$

where $u(t_i)$ are the horizontal displacements at the top (T) and bottom (B) nodes of the element at each time step t_i of the time history response and h is the storey height. We should note that, due to the low intensity of the 26-1-2014 earthquake, the interstorey drift ratios are well below the respective Seismic Code limits for the design or evaluation of structures, however they are useful in comparing the predictions of the three aforementioned scenarios.

From Table 2, we see that for the modeling case 2 (fixed-base structure excited by the actual LEF2 records), lower deformations (interstorey drift ratios) are predicted compared to SSI case 3, and may thus lead to a non-conservative design of the structure. Also, the aforementioned lower potential for building damage of the basement record (LEF2) with respect to the free-field record (LEF3) is reflected in the associated maximum drift ratios under the fixed-base scenario, which are lower under the LEF2 motion. Thus, the use of basement records, without appropriate corrections, in seismic hazard evaluations and the establishment of Ground Motion Prediction Equations may lead to unreliable results. This

Table 1 Ground motion parameters for recorded and computed response

Ground motion parameter	Recorded response X-dir EF2 (basement)	Predicted response FIM-CVLink (basement)	Recorded response X-dir LEF3 (free-field)	Recorded response Y-dir LEF2 (basement)	Predicted response FIM-CVLink (basement)	Recorded response Y-dir LEF3 (free-field)
Max acceleration (m/s)	0.22577	0.25358	0.27014	0.23637	0.32521	0.37868
Arias intensity (m/s)	0.01691	0.02441	0.02976	0.01947	0.02772	0.03350
Acceleration spectrum intensity (m/s)	0.21936	0.28290	0.32934	0.23474	0.32563	0.36824
Housner intensity (m)	0.12657	0.13621	0.13346	0.15332	0.15395	0.15261

Table 2 Maximum interstorey drift ratios (%) for various building supports and excitation scenarios

Direction under study	x-x				y-y				
	Fixed-base		Flexible-base (CVLink)		Fixed-base		Flexible-base (CVLink)		
Support conditions	3D FE	3D FE	3D FE	Simplified “stick” model	3D FE	3D FE	3D FE	Simplified “stick” model	
Structural model									
Base excitation	LEF3	LEF2	FIM	FIM	LEF3	LEF2	FIM	FIM	
Ground storey (location)	(A)	0.0041	0.0023	0.0024	0.0034	0.0050	0.0026	0.0049	0.0080
	(B)	0.0042	0.0022	0.0025		0.0056	0.0029	0.0051	
	(C)	0.0041	0.0022	0.0024		0.0049	0.0026	0.0048	
	(D)	0.0046	0.0026	0.0026		0.0047	0.0024	0.0044	
1st Storey (location)	(A)	0.0043	0.0022	0.0024	0.0066	0.0046	0.0024	0.0046	0.0149
	(B)	0.0042	0.0022	0.0024		0.0050	0.0026	0.0046	
	(C)	0.0044	0.0023	0.0024		0.0047	0.0024	0.0046	
	(D)	0.0041	0.0022	0.0022		0.0049	0.0025	0.0045	

is in agreement with earlier findings by Sotiriadis et al. (2019) and requires attention and further investigation in order to minimize all the undesirable repercussions of such an underestimation of the seismic hazard.

Although it does not alter the conclusions about the need for a careful use of recordings at the basement of buildings, it should be noted that according to Table 2, in the case of the flexible-base building, the interstorey drift ratios along the X and Y directions are markedly different, which is not the case for the fixed-base scenarios. This may be associated with the contribution of the rocking motion of the foundation to the overall seismic response of the structure, taking into account that the rocking stiffness of the foundation about the x-axis is quite lower than that about the y-axis, and hence may lead to a higher contribution to the translational deformation along the y-axis.

In Table 3, the modal analysis results for the flexible-base CVLink model are presented. The modal participating mass ratios for each mode refer to the percentage of the total mass that the particular mode activates along each translational (U_x , U_y , U_z) and about each rotational (R_x , R_y , R_z) global degree of freedom. For each mode, the cumulative percentage of activated mass up to the particular mode is also shown. In support to the different rocking-induced vibrational modes along the two axes of the examined structure, as can be seen from Table 3, the modal participating mass ratio for the fundamental mode for rocking about the x-axis R_x (Mode 5, at 0.1279 s) is $U_y = 15.458\%$ for the translational y-direction, while the corresponding one around the y-axis R_y (Mode 6, at 0.1190 s) is only $U_x = 2.339\%$ for the translational x-direction. For comparison, the respective modal analysis results for the fixed-base case are presented in Table 4. It is observed that SSI leads to an elongation of the building’s fundamental periods from $T_{fixed,X} = 0.1235$ s to $T_{SSI,X} = 0.2382$ s in the x-x direction and correspondingly from $T_{fixed,Y} = 0.1388$ s to $T_{SSI,Y} = 0.2216$ s in the y-y direction. Due to the mass distributed nature of the model, the modal participating mass ratios of the fundamental modes are significantly lower in the fixed-base case, and naturally there are no modes corresponding to rocking rotations around the x-x and y-y axes. For this reason, in all computations a direct integration (and not

Table 3 Eigenvalues and Modal Participating Mass Ratios for Flexible-base (CVLink) model

Mode	Period sec	individual			Sum			Individual			Sum		
		U_x %	U_y %	U_z %	ΣU_x %	ΣU_y %	ΣU_z %	R_x %	R_y %	R_z %	ΣR_x %	ΣR_y %	ΣR_z %
1	0.2382	95.839	0.000	0.000	95.839	0.000	0.000	0.005	1.669	0.280	0.005	1.669	0.280
2	0.2216	0.000	78.924	0.085	95.839	78.924	0.085	15.943	0.077	0.041	15.947	1.746	0.321
3	0.1632	0.212	0.113	0.000	96.050	79.037	0.085	0.090	0.065	88.399	16.038	1.811	88.721
4	0.1420	0.007	1.323	92.469	96.058	80.360	92.553	3.437	0.339	0.004	19.475	2.150	88.724
5	0.1279	0.202	15.458	4.760	96.260	95.817	97.313	71.375	11.002	0.077	90.850	13.152	88.801
6	0.1190	2.339	1.637	0.019	98.599	97.455	97.332	3.871	78.565	0.016	94.721	91.717	88.817
7	0.0890	1.324	0.205	0.002	99.922	97.660	97.335	0.144	3.641	0.002	94.865	95.358	88.820
8	0.0846	0.028	2.246	0.028	99.951	99.906	97.362	2.404	0.317	0.023	97.268	95.675	88.842
9	0.0807	0.023	0.000	0.001	99.973	99.906	97.363	0.011	0.001	10.958	97.279	95.676	99.800
10	0.0769	0.000	0.000	0.003	99.973	99.906	97.366	0.001	0.001	0.001	97.281	95.678	99.801

modal) time-history scheme was applied, which is particularly important especially for the fixed-base model. It must also be noted that, an additional analysis (not shown in Table 2) performed by assuming the model as fixed-based and subjected to the FIM excitation, yielded also a difference in the interstorey drifts between the X and Y directions, although not as pronounced as for the flexible-base model (in the order of $MIDR_X = 0.0026\%$ and $MIDR_Y = 0.0034\%$ for the ground storey and $MIDR_X = 0.0024\%$ and $MIDR_Y = 0.0031\%$ for the 1st storey).

5.2 Comparison of 3D vs simplified F.E. building model

In the following, the response of a simplified lumped-mass Multi-Degree-of-Freedom (MDOF) “extensive stick” model (Fig. 17) developed in Karakostas et al. (2017) is compared against full 3D model of the building under flexible-base conditions. Details on the development and properties of this simplified model can be found in the above reference. To this end, the link element involving the point springs and dashpots computed above (CVLink) was also attached to the base of the simplified model. Thus, soil compliance is taken into account in the same manner between the two models, allowing for the investigation of the SSI response as affected solely by different considerations for structural modeling. A modal analysis of the flexible-base simplified model resulted in a fundamental period of 0.2592 s in the $x-x$ and 0.2657 s in the $y-y$ direction, which are somewhat higher than the fundamental periods obtained from the 3D model (Table 3).

In Fig. 18, a comparison is made between the computed response of the building at the location of the accelerometer sensor at its basement by the full 3D model against the simplified one. At first sight, one may deem that the predictions of the simplified model are acceptably near (from an engineering point of view) to those of the full 3D one (although some discrepancies are observed especially along the Y–Y direction in the frequency domain). However, one must take into account that the computed response is made for the location of the sensor at the basement, i.e. at a very short height (around 0.9 m) from the base of the building. At that height, the inertial amplification of the FIM due to each model’s dynamic response is rather small (especially since the basement floor is rigid by construction (Fig. 9b)), and hence, the discrepancies between the predictions of the two models are rather small to observe. However, this is not the case for the response at other locations of the building.

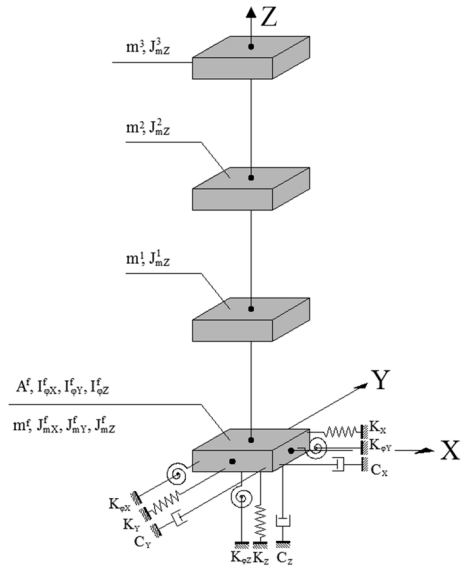
The discrepancies become more significant at higher locations of the superstructure, as it becomes obvious through the comparison of the maximum interstorey-drift ratios at the ground and first storey levels predicted by the simplified “stick” model vs the full 3D one, which are presented in Table 2. As can be seen, the simplified model substantially over-predicts the drift ratios (by a factor of around 1.4 for the ground, and of around 3 for the first storey, in both the $x-x$ and $y-y$ directions). This can be attributed to the fact that the simplified model is somewhat more flexible than the 3D one, but mainly that it lacks the information of the spatial distribution of the earthquake-resisting elements (columns and shear walls), which contribute to the overall lateral resistance both through their individual geometric and material properties, as well as their specific spatial location in the structural system.

The above comparisons highlight the importance of using, instead of simplified one, a full 3D, mass-distributed FE model of the building, that allows a more refined assessment of structural response as affected by SSI under earthquake loading, especially when the geometry of the building is not regular (i.e. elongated dimensions, holes in plan, possibility

Table 4 Eigenvalues and modal participating mass ratios for fixed-base model

Mode	Period sec	Individual			Cumulative			Individual			Cumulative		
		U_x %	U_y %	U_z %	ΣU_x %	ΣU_y %	ΣU_z %	R_x %	R_y %	R_z %	ΣR_x %	ΣR_y %	ΣR_z %
1	0.1388	0.088	49.991	0.004	0.088	49.991	0.004	18.953	0.008	0.313	18.953	0.008	0.313
2	0.1235	45.534	0.089	0.006	45.622	50.080	0.010	0.024	6.464	0.014	18.977	6.472	0.327
3	0.1164	0.037	0.160	0.003	45.659	50.240	0.013	0.062	0.002	45.969	19.038	6.473	46.296
4	0.0769	0.001	0.000	0.065	45.660	50.240	0.078	0.002	0.018	0.000	19.041	6.491	46.296
5	0.0759	0.002	0.000	0.005	45.662	50.240	0.083	0.003	0.022	0.000	19.044	6.513	46.296
6	0.0751	0.027	0.001	0.219	45.688	50.241	0.303	0.160	0.000	0.002	19.204	6.514	46.298
7	0.0747	0.000	0.003	0.020	45.688	50.243	0.322	0.045	0.002	0.003	19.249	6.516	46.301
8	0.0738	0.010	0.000	1.071	45.699	50.244	1.393	0.047	2.689	0.001	19.296	9.205	46.302
9	0.0722	0.006	0.000	0.047	45.705	50.244	1.440	0.075	0.019	0.001	19.371	9.224	46.303
10	0.0709	0.000	0.000	0.818	45.705	50.244	2.258	0.491	0.939	0.006	19.863	10.162	46.309

Fig. 17 Simplified “extensive stick” model of the building (from Karakostas et al. 2017)

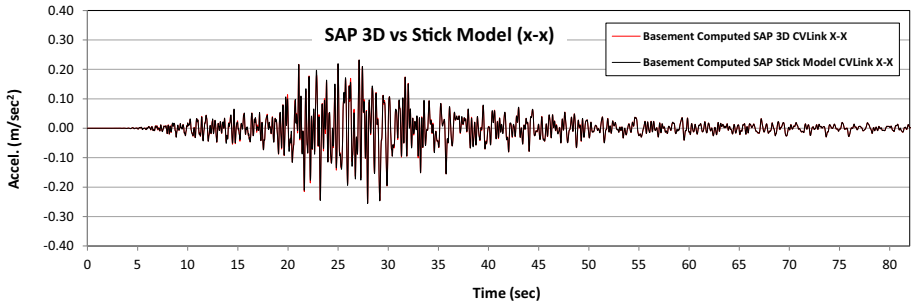


of torsional effects etc.) like the one examined herein. In such cases, the use of an equivalent simplified model may not be appropriate and should be made with caution.

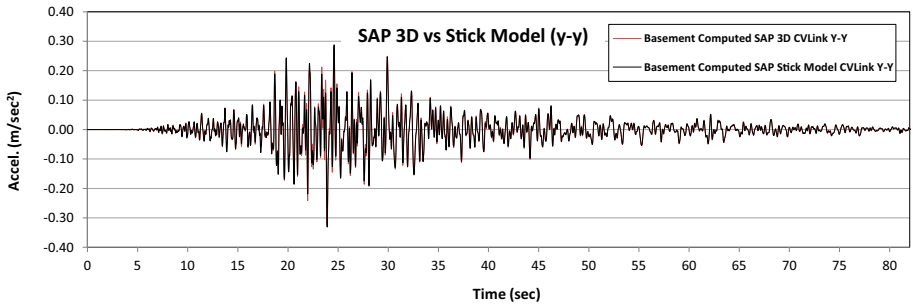
6 Conclusions

A numerical investigation of the Lefkada Regional Administration building’s response recorded during the M6.1, January 26, 2014 Cephalonia earthquake was performed by implementing the substructure approach to model the coupled soil-foundation-structure system and explore SSI effects. For the inertial part of the interaction mechanism, a refined 3D, mass-distributed Finite Element model supported on point springs and dashpots was formed to model the superstructure on flexible supports, while kinematic interaction effects were considered by means of well-known analytical expressions that have been reported for the assessment of the Foundation Input Motion (FIM).

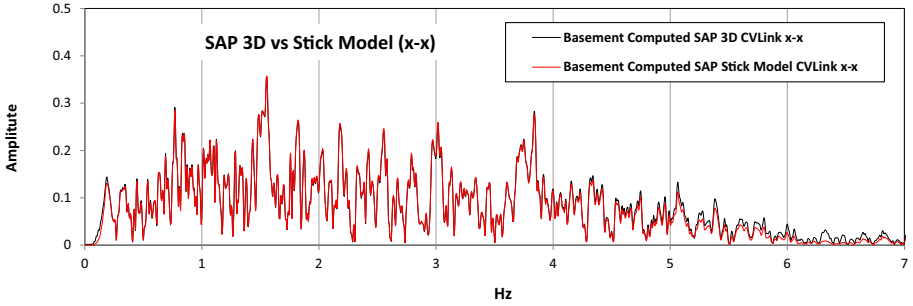
The prediction of the recorded response at the basement of the building was satisfactory, from an engineering point of view. However, a kinematic dominated response of the foundation characterized by strong filtering of the free-field motion was revealed from the processed signals. This aspect was not adequately captured by the analytical expressions under consideration, leading to an overestimated prediction of the actual response in a certain frequency range. A serious issue that was also explored referred to the direct use, in the design of new buildings considered as fixed-base, of recordings from sensors being installed at the basement of buildings, which is not explicitly restricted by the Seismic Code, in absence of free-field recordings. It was shown that this leads to an underestimation of the expected response compared to a more accurate approach that models SSI effects, and thus to a non-conservative design of the structures. On the other hand, the direct use of actual free-field recordings under the assumption of fixed-base structure, leads to a conservative design. In general, basement recordings have a lower potential for building damage compared to free-field ones, and their use, without appropriate corrections, for the design of buildings or for seismic hazard



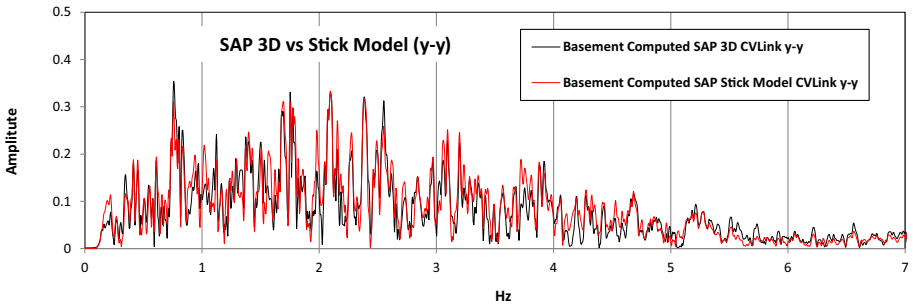
(a)



(b)



(c)



(d)

Fig. 18 Computed response at the location of the sensor recorder 3D vs Stick model

evaluations and development of Ground Motion Prediction Equations may lead to unconservative results. Finally, comparison of results between the herein developed full 3D model and a simplified lumped-mass MDOF model, points out the importance of using detailed F.E. models of a structure, especially when its geometry deviates from a regular one.

Funding The authors declare no funding for the presented research.

Availability of data and material The data that support the findings of this study are available from the corresponding author, Christos Karakostas, upon reasoned request.

Declarations

Conflict of interest The authors declare that they have no conflict of interest or competing interests.

References

- ASCE (2007) Seismic rehabilitation of existing buildings. ASCE standard ASCE/SEI 41-06. American Society of Civil Engineers. Virginia
- ATC (2005) Improvement of nonlinear static seismic analysis procedures. Rep. No. FEMA-440. Federal Emergency Management Agency, Washington, D.C
- Avramidis I, Athanatopoulou A, Morfidis K, Sextos A, Giaralis A. (2016) Eurocode-compliant seismic analysis and design of R/C buildings: concepts, commentary and worked examples with flowcharts. Geotechnical, geological and earthquake engineering. Springer, New York
- Bielak J (1975) Dynamic behavior of structures with embedded foundations. *Earthq Eng Struct Dyn* 3:259–274
- Conti R, Morigi M, Viggiani GMB (2017) Filtering effect induced by rigid massless embedded foundations. *Bull Earthq Eng* 15(3):1019–1035
- Conti R, Morigi M, Rovithis E, Theodoulidis N, Karakostas C (2018) Filtering action of embedded massive foundations: New analytical expressions and evidence from two instrumented buildings. *Earthq Eng Struct Dyn* 47(5):1229–1249
- Dai K, Dan L, Zhanga S, Shia Y, Mengc J, Huangd Z (2020) Study on the damping ratios of reinforced concrete structures from seismic response records. *Eng Struct* 223:111143
- Di Laora R, de Sanctis L (2013) Piles-induced filtering effect on the foundation input motion. *Soil Dyn Earthq Eng* 46:52–63
- EAK2000 (2000) Greek National Seismic Code
- EKOS2000 (2000) Greek National Reinforced Concrete Code
- Elsabee F, Morray JP (1977) Dynamic behavior of embedded foundation. Rep. No. R77-33, Dept. of Civil Engineering, Massachusetts Institute of Technology, Cambridge, Mass
- Gazetas G, Mylonakis G (1998) Seismic soil-structure interaction: new evidence and emerging issues. *Geotech Earthq Eng Soil Dyn III* 2:1119–1174
- Gazetas G (1991) Formulas and charts for impedances of surface and embedded foundations. *J Geotech Eng* 117(9):1363–1381
- Givens MJ, Mikami A, Kashima T, Stewart JP (2012) Kinematic soil-structure interaction effects from building and free-field seismic arrays in Japan. In: Proceedings of the joint conference 9th international conference of urban earthquake engineering and 4th Asia conference on earthquake engineering, Tokyo, Japan
- Iovino M, Di Laora R, Emm R, de Sanctis L (2019) The beneficial role of piles on the seismic loading of structures. *Earthq Spectra* 35(3):1141–1162
- Karakostas C, Kontogiannis G, Morfidis K, Rovithis E, Manolis G, Theodoulidis N (2017) Effect of soil-structure interaction on the seismic response of an instrumented building during the Cephalonia, Greece earthquake of 26-1-2014. In: Papadrakakis M, Fragiadakis M (eds) Proceedings of COMP-DYN 2017, 6th ECCOMAS thematic conference on computational methods in structural dynamics and earthquake engineering. Rhodes Island, Greece, 15–17 June
- Kausel E, Whitman RV, Morray JP, Elsabee F (1978) The spring method for embedded foundations. *Nucl Eng Des* 48:377–392

- Kramer SL (1996) Geotechnical earthquake engineering. Prentice-Hall
- Kim S, Stewart JP (2003) Kinematic soil-structure interaction from strong motion recordings. *J Geotech Geoenviron Eng* 129(4):323–335
- Makris N, Gazetas G, Delis G (1996) Dynamic soil-pile-foundation-structure interaction: records and predictions. *Géotechnique* 46(1):33–50
- Mikami A, Stewart JP, Kamiyama M (2008) Effects of time series analysis protocols on transfer functions calculated from earthquake recordings. *Soil Dyn Earthq Eng* 28:695–706
- Mylonakis G, Gazetas G (2000) Seismic soil-structure interaction: beneficial or detrimental? *J Earthq Eng* 4(3):377–401
- Mylonakis G, Nikolaou S, Gazetas G (2006) Footings under seismic loading: analysis and design issues with emphasis on bridge foundations. *Soil Dyn Earthq Eng* 26(9):824–853
- National Institute of Standards and Technology (NIST) (2012) Soil-structure interaction for building structures. Report NIST GCR 12-917-21. USA: NEHRP Consultants Joint Venture
- Pandey BH, Liam Finn WD, Ventura CE (2012) Modification of free-field motions by soil-foundation-structure interaction for shallow foundations. In: Proceedings of 15th world conference on earthquake engineering. Lisbon, 24–28 September, paper 3575
- Poland C, Sun J, Meija L (2000) Quantifying the effect of soil-structure interaction for use in building design. Data utilization report CSMIP/00-02. California Department of Conservation, CA
- Rathje EM, Abrahamson NA, Bray JD (1998) Simplified frequency content estimates of earthquake ground motions. *J Geotech Geoenviron Eng* 124(2):150–159
- SAP2000® (2000) Structural analysis program. Computers & Structures Inc., 1976–2021
- Sotiriadis D., Klimis N., Margaris B. and Sextos A. (2020) Analytical expressions relating free-field and foundation ground motions in buildings with basement, considering soil-structure interaction. *Engineering Structures*, 216;110757.
- Sotiriadis D, Klimis N, Margaris B, Sextos A (2019) Influence of structure—foundation—soil interaction on ground motions recorded within buildings. *Bull Earthq Eng* 17:5867–5895
- Stewart JP (2000) Variations between foundation-level and free-field earthquake ground motions. *Earthq Spectra* 16(2):511–532
- Theodoulidis N, Karakostas Ch, Lekidis V, Makra K, Margaris B, Morfidis K, Papaioannou Ch, Rovithis E, Salonikios Th, Savvaidis A (2016) The Cephalonia, Greece, January 26 (M6.1) and February 3, 2014 (M6.0) earthquakes: near-fault ground motion and effects on soil and structures. *Bull Earthq Eng* 14(1):1–38
- Trifunac MD, Hao TY, Todorovska MI (2001) Response of a 14-story reinforced concrete structure to nine earthquakes: 61 years of observation in the Hollywood Storage Building. Rep. No. CE 01–02, Dept. of Civil Engineering, University of Southern California
- Veletsos AS, Meek JW (1974) Dynamic behaviour of building-foundation systems. *Earthq Eng Struct Dyn* 3:121–138
- Veletsos AS, Prasad AM, Wu WH (1997) Transfer functions for rigid rectangular foundations. *Earthq Eng Struct Dyn* 26:5–17

Publisher's Note Springer Nature remains neutral with regard to jurisdictional claims in published maps and institutional affiliations.

Authors and Affiliations

Christos Karakostas¹  · Konstantinos Morfidis¹  · Emmanouil Rovithis¹  · Nikolaos Theodoulidis¹ 

Konstantinos Morfidis
kmorfidis@itsak.gr

Emmanouil Rovithis
rovithis@itsak.gr

Nikolaos Theodoulidis
ntheo@itsak.gr

¹ Institute of Engineering Seismology and Earthquake Engineering (EPPO-ITSAK), Dasiliou Str., Eleones, Pylaia, 55535 Thessaloniki, Greece